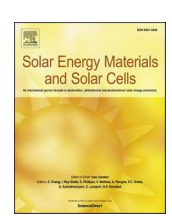
ELSEVIER

Contents lists available at ScienceDirect

Solar Energy Materials and Solar Cells

journal homepage: www.elsevier.com/locate/solmat





Selenium passivates grain boundaries in alloyed CdTe solar cells

Thomas Fiducia ^{a,*}, Ashley Howkins ^b, Ali Abbas ^a, Budhika Mendis ^c, Amit Munshi ^d, Kurt Barth ^d, Walajabad Sampath ^d, John Walls ^a

- ^a Loughborough University, Leicestershire, LE11 3TU, UK
- ^b Brunel University London, Uxbridge, UB8 3PH, UK
- ^c Durham University, Durham, DH1 3LE, UK
- ^d Colorado State University, Fort Collins, CO, USA

ARTICLE INFO

Keywords: Cadmium telluride Grain boundaries Selenium TEM Cathodoluminescence

ABSTRACT

Cadmium telluride (CdTe) solar cells have achieved efficiencies of over 22%, despite having absorber layer grain sizes less than 10 μ m and hence a very high density of grain boundaries. Recent research has shown that this is possible because of partial passivation of grain boundaries during the widely used cadmium chloride treatment, and passivation of grain interior defects by selenium alloying of the CdTe. Here, state-of-the art TEM-based cathodoluminescence imaging is used to show that, in addition to grain interiors, selenium also passivates grain boundaries in alloyed Cd(Se_x,Te_{1-x}) material (CST). Specifically, we find that recombination at CST grain boundaries is up to an order of magnitude lower than at CdTe grain boundaries. This further explains the superior performance of selenium graded CdTe devices and provides potential new routes for further efficiency improvement and solar electricity cost reduction.

1. Introduction

In the last decade, the efficiency of cadmium telluride (CdTe) solar cells has risen from 16.7% to the current record of 22.1% [1–3]. This is significantly higher than for the best polycrystalline gallium arsenide cells at 18.4%, and near the record for multi-crystalline silicon cells at 22.3%, despite the fact that CdTe grains are more than 1,000 times smaller than silicon grains by diameter [3–5] (CIGS devices, which also have small grain sizes, have reached efficiencies of 23.35% [3]). Three discoveries in CdTe solar cell research have helped to explain the high CdTe device performance, despite its fast-grown, high defect density absorber material, all of which relate to the introduction of either chlorine or selenium into the CdTe.

Firstly it was found that during the cadmium chloride (CdCl₂) heat treatment, which is used universally to produce high efficiency CdTe cells, chlorine segregates to grain boundaries in the CdTe and partially passivates them [6–10]. Barnard et al. then showed that in addition to grain boundaries, the treatment also increases carrier lifetimes in the interiors of CdTe grains, and at the front interface of the absorber [11–13]. Finally, in 2019 our group used SEM-based cathodoluminescence (SEM-CL) to show that selenium, which was initially alloyed with CdTe at the front of the absorber layer to decrease its

bandgap, also has a passivation effect on grain interiors in both treated and untreated CST [14,15]. This helped to explain the superior opto-electronic properties of polycrystalline CST, which can have higher carrier lifetimes than even single-crystal CdTe (750 ns, vs 670 ns for the best single crystal CdTe [16,17]). However, while the SEM-CL data clearly showed the positive effects of selenium in the interiors of CST grains, it did not show whether it affects recombination at grain boundaries. Low contrast defects such as passivated grain boundaries are hard to resolve in SEM-CL, since it the width of the electron beam-sample interaction volume is more than 250 nm in CdTe, even at high resolution beam settings (7.5 keV beam energy, with 75% of carriers generated within this volume [18]).

The effects of selenium on the electronic properties of CdTe grain boundaries has been modelled in several recent papers using density functional theory (DFT). Calculations by Guo et al. [19,20] suggested that co-doping of selenium and chlorine at a CdTe dislocation core reduced the density of mid-gap states associated with the defect. Modelling by Wei et al. [21] suggested that selenium segregates to Te-core CdTe grain boundaries, substitutes with tellurium, and reduces the depth and density of mid-gap states. And most recently, Shah et al. [22] modelled chlorine and selenium at a CdTe grain boundary and concluded that together the elements reduced the density of harmful

E-mail address: T.A.M.Fiducia@lboro.ac.uk (T. Fiducia).

^{*} Corresponding author.

mid-gap defect states.

Despite this modelling work, real-world evidence of CdTe grain boundary passivation with selenium is limited. In 2019, Zheng et al. [23] performed time-resolved PL mapping on a bilayer CST/CdTe device and found that carrier lifetimes were more homogeneous (and higher) in the CST layer than the CdTe, suggesting lower levels of grain boundary recombination in the CST. And recently, in 2021, Amarasinghe et al. [24] performed SEM-CL mapping on separate, test CST and CdTe double heterostructures and found that the drop in luminescence intensity at CST grain boundaries was lower than at CdTe grain boundaries.

Here, we assess the electronic effects of selenium on grain boundaries in a working bilayer CST/CdTe device (efficiency 16.8%) using high resolution CL imaging in a scanning transmission electron microscope (STEM-CL) [25]. Whereas high resolution STEM-CL imaging of a solar cell has previously not been achieved because of problems with low signal, we use cryogenic cooling of the TEM foil and xenon ion milling of the sample to boost the CL signal and overcome this issue [26]. Using STEM-CL allows us to directly correlate the CL maps to TEM micrographs of the absorber layer microstructure and high-resolution STE-M-EDX maps of elemental composition, which is a key benefit of the TEM-based technique. The results provide direct evidence that selenium has a passivation effect on grain boundaries in alloyed CST material – on top of what can be achieved with chlorine alone. This further explains how polycrystalline selenium-graded CdTe devices can compete on efficiency with large-grained, slow-grown, and more expensive competitors like silicon [27].

To perform the investigation, two bilayer CST/CdTe solar cells were fabricated at Colorado State University as described in the methods section. One of the samples was left as-deposited while the other received a cadmium chloride (CdCl₂) heat treatment. Cross-sectional TEM foils (~125 nm thick) were then ion milled and 'lifted out' from the samples. Crucially, in order to maximise the luminescence signal from the foils, the ion milling was performed using a xenon focused ion beam (FIB), as opposed to the traditional gallium FIB. Because of the higher atomic mass of xenon there is less implantation of ions into the foil during milling. This reduces the number of harmful point defects that are introduced to the sample, reducing the number of non-radiative recombination channels available to carriers and therefore increasing

the luminescence signal. In addition, because xenon is inert, the defects that are formed are less likely to be harmful than those created by gallium implantation. To confirm the superior electronic properties of xenon milled CdTe compared to gallium milled material, we ion milled two bevelled trenches adjacent to each other in a CdTe film, one with a xenon beam and one with a gallium beam and compared the SEM-CL signal from the two bevels. The results are shown in Fig. S1 in the supplementary information. It can be seen that the CL signal from the Ga milled bevel is significantly lower than the signal from the Xe milled bevel. Moreover, the level of CL signal from the xenon milled bevel is similar to that from the unprepared CdTe surface either side of the trench, showing that xenon ion milling introduces minimal defects compared to an unprepared CdTe surface.

In addition to using a Xe milled lamella, another way to improve the luminescence signal from a sample is to cryogenically cool it down, as this increases the efficiency of radiative recombination. As such, during the STEM-CL measurements, liquid nitrogen was used to cool the lamellae to approximately $-170\,^{\circ}\text{C}.$ We found cooling to be particularly important, and without it, the CL signal was very low even with a xenon ion milled sample.

2. Results

2.1. As-deposited device

A cross-sectional TEM micrograph of the as-deposited CST/CdTe bilayer device is shown in Fig. 1a. Generally, small columnar grains are seen in the CST layer, and larger grains in the CdTe. However, there are some instances where the CdTe has grown epitaxially on the CST material and formed continuous grains that span the two layers (see dashed lines in the figure). The distribution of selenium within the cross-section is shown in the STEM-EDX map in Fig. 1b. It shows that selenium (\sim 10 at%) is contained within the CST layer, with no detectable diffusion into the CdTe during deposition [28]. This is mirrored by the tellurium EDX signal distribution in Fig. 1c, which shows higher tellurium signal in the CdTe and lower signal in the CST as expected.

The cathodoluminescence signal distribution over the bilayer is shown in Fig. 1d. In the CdTe region at the top of the absorber, the CL

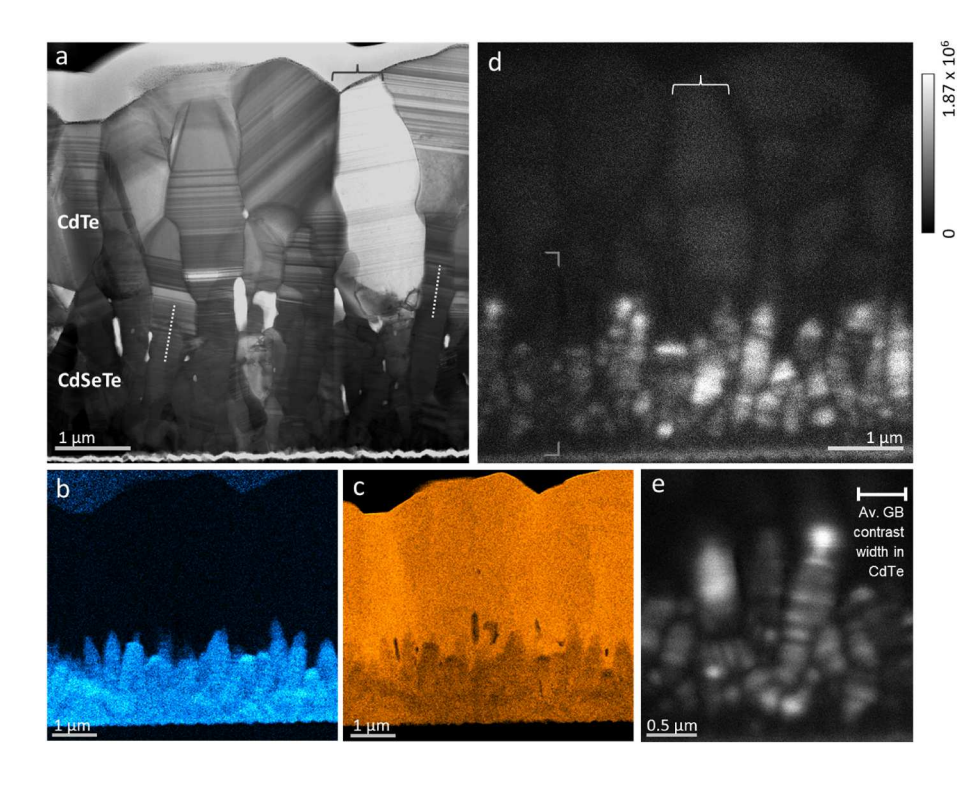


Fig. 1. (a) Cross-sectional TEM micrograph of the asdeposited CST/CdTe device, with dashed lines showing where CdTe has grown epitaxially on CST grains. (b) EDX map of the selenium signal distribution over the cross-section, with brighter blue showing higher signal. (c) EDX map of the tellurium signal distribution over the cross section, with brighter orange showing higher signal. (d) Lowtemperature STEM-based cathodoluminescence (CL) map (-169.3 °C) of the luminescence signal over the cross-section, with the field of view shifted slightly from that in (a) (the brackets in (a) and (d) show the same grain). The corner annotations show the region where the higher magnification image in (e) was taken. The intensity scale bar shows backgroundsubtracted counts. (e) Higher magnification image of the CL intensity variations over a region in the CST layer. The measure in the top right of the image shows the average contrast width of the CdTe grain boundaries at this magnification. (For interpretation of the references to colour in this figure legend, the reader is referred to the Web version of this article.)

signal is low, with counts in the grain interior (2.65×10^6) barely reaching higher than the background level, taken from the platinum region of the lamella (2.39×10^6). This is expected because it is known that as-deposited CdTe material has a low luminescence efficiency, particularly compared to CdCl₂ treated CdTe [11,29,30]. However, there is sufficient signal to distinguish dark contrast at the CdTe grain boundaries, which is due to increased non-radiative carrier recombination at grain boundary defects (dangling bonds, wrong bonds, etc) compared to the grain bulk.

In the CST layer, the cathodoluminescence signal is significantly brighter than in the CdTe, despite the smaller CST grains (background-subtracted counts reach $\sim\!1.8\times10^6$ in the CST, compared to a maximum of $\sim\!0.26\times10^6$ in the CdTe). This is consistent with our recent SEM-based CL results which show that selenium alloying significantly increases luminescence efficiency within the grain bulk of both treated and untreated CST material [14,15]. Values of grain boundary contrast in the CST and CdTe are similar at $\sim\!50\%$, however the width of the grain boundary contrast in the CST is only $\sim\!250\text{--}300$ nm, compared to an average contrast width of $\sim\!500$ nm in the CdTe (shown to scale on the image for comparison).

As well as dark contrast between grains, there are also signal variations within grains in the CST layer. These are shown more clearly in the higher magnification image in Fig. 1e, where it can be seen that the signal variations are bands of brighter and darker contrast within the CST grains. Comparison with the TEM micrographs shows that these bands run parallel to the (111) twinning plane of the grains, indicating that the in-grain signal variations are caused by twinning of the CST. This could be due to increased carrier recombination at regions of highly faulted or hexagonal phase material, or to variations in the defect density at different crystal facets (111, 100, etc) which are exposed during the milling of the TEM lamella surfaces, and which are affected by twinning [15].

2.2. Cadmium chloride treated device

A TEM micrograph of the cadmium chloride treated CST/CdTe device is shown in Fig. 2a. In contrast to the untreated device, which has a bilayer structure, there are no distinct CST and CdTe layers in the treated absorber and grain sizes are generally larger. This shows that there has

been recrystallisation of the absorber layer during the cadmium chloride heat treatment. An EDX map of the selenium signal distribution in the cross-section is shown in Fig. 2b, and in Fig. 2c this map has been superimposed on top of the TEM micrograph. Compared to the untreated device, the maps show a more gradual decrease in selenium signal from the front to the back of the film. This indicates that during the CdCl₂ treatment, selenium diffuses from the CST layer into the CdTe [31]. In the interdiffused region between the top and bottom of the film, higher selenium signal is seen at grain boundaries compared to the adjacent bulk (e.g. circled grain boundary in Fig. 2b), indicating that grain boundaries provide a pathway for preferential diffusion of selenium into the CdTe layer [28]. The EDX map for chlorine is shown in Fig. 2e and indicates segregation along the grain boundaries, consistent with previous reports [7,8,28]. In Fig. 2e there appears to be less chlorine segregation at some grain boundaries in the CdTe region at the top of the film. This is an experimental artefact caused by the large inclination of these grain boundaries within the TEM foil (see Fig. 2a), resulting in a large GB projected width and therefore less sensitivity of the measured EDX signal to chlorine segregation. CdTe grain boundaries that are close to being 'end-on' (e.g. the arrowed grain boundary in Fig. 2e) show the expected chlorine signal enhancement. Furthermore, EDX measurements on different regions of the sample show that chlorine is present along grain boundaries throughout the film thickness (see Fig. S4).

A STEM-CL map acquired on the device cross-section is shown in Fig. 2d. Unlike in the untreated device, the CL signal in the grain interior of the CdTe is significantly higher than the background counts, measured at the platinum layer (2.34 x10⁶ background counts vs 3.05 x10⁶ counts in the CdTe). Although counts between different samples are not directly comparable, this suggests that grain interior luminescence in the treated CdTe is higher than in the untreated device. Higher grain interior signal enables clear grain boundary contrast to be seen in the treated sample. However, there is significant variation in the amount of contrast at grain boundaries depending on their depth through the absorber. In the CdTe region towards the top of the film there are thick, dark bands of grain boundary contrast. At the bottom of the film, in the CST material, there are only thin, faint lines of contrast (see the solid arrowed grain boundary in the figure). For instance, the width of GB contrast in three of the CdTe boundaries in the image are all between 500 and 600 nm, with a grain boundary contrast of between 63 and

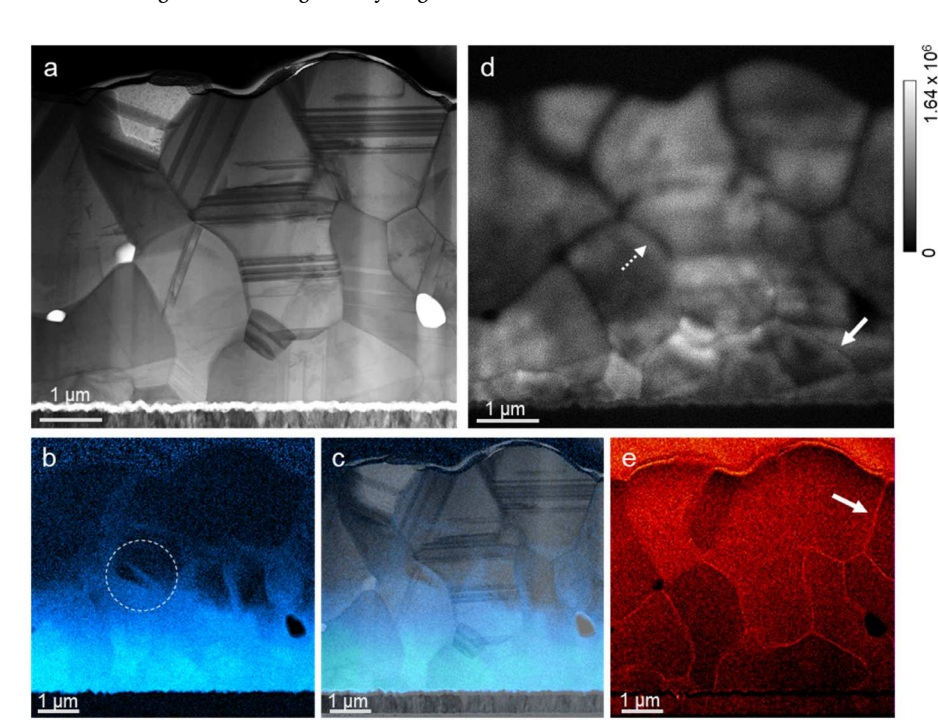


Fig. 2. (a) Cross-sectional bright field TEM micrograph of the cadmium chloride treated CST/CdTe device. (b) EDX map of the selenium distribution in the cross section (brighter blue shows higher selenium signal intensity). (c) Map of the selenium signal distribution in (b), superimposed on top of the micrograph in (a). (d) Low-temperature STEM-based cathodoluminescence (CL) map (-170.6 °C) of the panchromatic CL intensity over the cross-section, with arrows highlighting the thinner grain boundary contrast in the interdiffused region (dashed arrow) and CST (solid arrow) versus the CdTe. Intensity scale bar shows background-subtracted counts, with the background taken at the platinum region above the CdTe. (e) EDX map of the chlorine signal intensity over the cross-section. The arrow shows an 'edge on' grain boundary in the CdTe. (For interpretation of the references to colour in this figure legend, the reader is referred to the Web version of this article.)

78%. This means that the background-corrected signal at the trough of the V-shaped CL profile is 63-78% lower than the averaged, background-corrected signal on both sides of the boundary (see the CL profile in Fig. S2 in the Supplementary Information for example). This compares to the solid arrowed boundary in the CST, where the GB contrast is only 29%, with a width of 100 nm (see Supplementary Fig. S2). This reduction in grain boundary contrast and width shows that there is significantly lower carrier recombination in the CST grain boundaries compared to CdTe. Since the bilayer has been CdCl₂ treated, this is 'extra' GB passivation - on top of what can be achieved with only chlorine at the grain boundaries. In addition, the data shows that the level of grain boundary passivation is generally dependent on the amount of selenium at each boundary. For instance, a boundary with an intermediate concentration of selenium around it has been circled in the selenium map in Fig. 2b. It can be seen in the CL map (dashed arrow) that the contrast at this boundary is also intermediate, i.e lower than that at pure CdTe boundaries, but higher than at boundaries in the CST. This indicates that for the selenium concentration ranges present in this cell (0-10 at%), the more selenium that is present at and around a boundary, the greater the passivation of the boundary.

It is possible to extract the recombination velocity of individual grain boundaries from CL images, as has previously been demonstrated for SEM-CL [32]. The CL contrast $\Delta I(x)$ at a distance x from the grain boundary is given by Ref. [32]:

$$\log[\Delta I(x)] = \log\left(\frac{S_{red}}{S_{red} + 1}\right) - \frac{x}{L}$$
(1)

where L is the minority carrier diffusion length and S_{red} is the reduced recombination velocity. S_{red} is related to the grain boundary recombination velocity (S) by $S_{red} = S\tau/L$, where τ is the carrier lifetime. By plotting $log[\Delta I(x)]$ as a function of x, the diffusion length L and reduced recombination velocity S_{red} can be extracted. The CL contrast is defined as $\Delta I(x) = 1 - [I(x)/I_o]$, where I(x) is the CL intensity at distance 'x' from the grain boundary and I_o is the plateau CL intensity at the grain interior [32]. The CL intensities were background subtracted prior to analysis (the background was defined using the platinum layer).

In this model it is assumed that free surface recombination can be ignored. While this can be approximately satisfied in SEM by increasing the energy of the incident beam, it is not possible to ignore surface recombination in TEM-CL. Despite this, a recent TEM-CL study by Yoon et al. [33] has shown that Equation (1) can still be applied, provided the lifetime τ is replaced by an effective lifetime τ_{eff} that is lower than the bulk value. τ_{eff} is determined by surface recombination and is a function of the TEM specimen thickness. The effective diffusion length is then $L_{eff} = \sqrt{(D\tau_{eff})}$, where D is the carrier diffusion coefficient.

Applying Equation (1) to our TEM-CL data would yield effective values for the diffusion length and reduced recombination velocity. Since these values depend on the specimen thickness they are not very useful on their own. However, it does enable us to compare different grain boundaries provided the data are all extracted from the same specimen. Fig. 3a shows the TEM-CL map (same as Fig. 2d) with the analysed grain boundaries indicated in numerical order. Three CdTe and three CST grain boundaries were found to be suitable for quantitative analysis. Fig. 3b shows an example CL intensity profile across a grain boundary and Fig. 3c its linearisation according to Equation (1). The linearisation plots for the grain boundaries all had a regression coefficient larger than 0.95, apart from grain boundary 5 which had a lower regression coefficient of 0.87. When selecting CST grain boundary profiles, care was taken to ensure the selenium concentration was uniform over the region of interest; this was done by comparing with the EDX map for selenium (Fig. 2b).

The effective diffusion length and recombination velocity values for CdTe and CST grain boundaries are listed in Tables 1 and 2 respectively.

Table 1Effective diffusion length and reduced recombination velocity values for CdTe grain boundaries (numbers 1 to 3 in Fig. 3a).

Grain boundary	Effective diffusion length L_{eff} (μm)	Reduced recombination velocity \mathbf{S}_{red}
1	0.13 ± 0.01	34.84 ± 127.35
2	0.16 ± 0.01	41.00 ± 94.71
3	0.13 ± 0.01	$\textbf{4.70} \pm \textbf{2.25}$

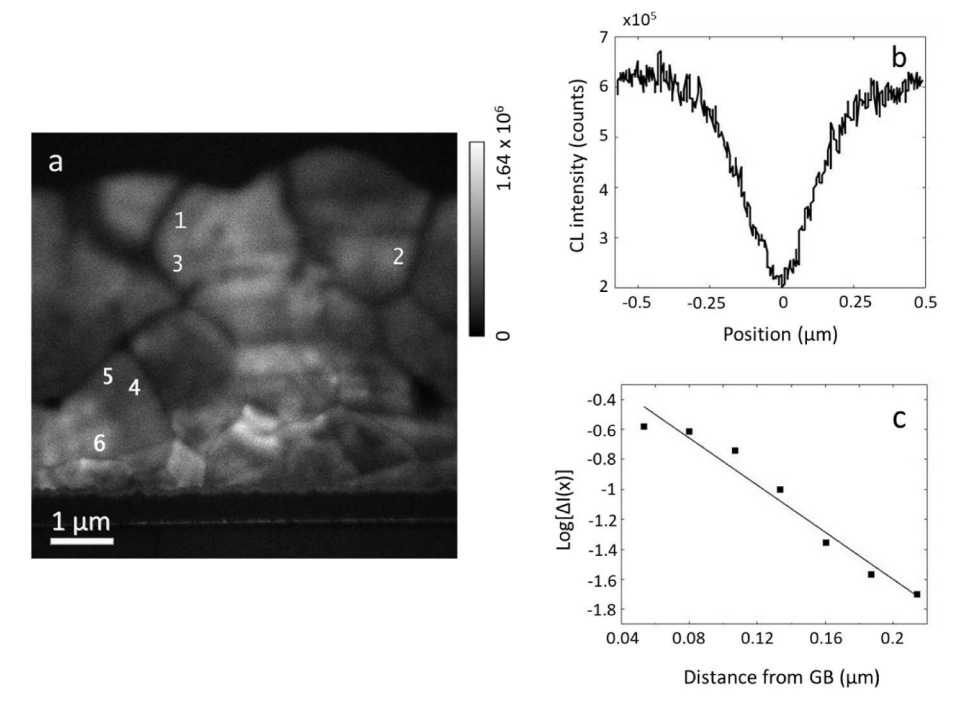


Fig. 3. (a) TEM-CL image of the treated bilayer device with the analysed grain boundaries indicated in numerical order. (b) shows the CL intensity profile across one of the grain boundaries (grain boundary 1) and (c) is its linearisation according to Equation (1).

Table 2 Effective diffusion length and reduced recombination velocity values for CST grain boundaries (numbers 4 to 6 in Fig. 3a).

Grain boundary	Effective diffusion length L_{eff} (μm)	Reduced recombination velocity $\boldsymbol{S}_{\text{red}}$
5	0.10 ± 0.01	5.64 ± 0.02
6	0.15 ± 0.03	1.42 ± 0.19
7	0.07 ± 0.01	0.83 ± 0.14

The average value for the effective diffusion length in CST is slightly smaller than CdTe, i.e. 0.11 μm vs 0.14 μm . Since $L_{eff} = \sqrt{(D\tau_{eff})}$ this could be due to differences in $\tau_{\rm eff}$ as well as the diffusion coefficient D between CdTe and CST regions. The TEM-CL measurements are strongly influenced by surface recombination and are performed at liquid nitrogen temperature. Therefore, the effective diffusion lengths reported here must not be confused with the bulk diffusion lengths that are relevant for room temperature photovoltaic device operation. Furthermore, Monte-Carlo simulations have shown that the steady-state carrier distribution volume within a 100 nm thick, CdTe TEM foil is only slightly smaller than the ~0.13 μm average effective diffusion length [26], i.e. the carrier concentration drops to 50% of its maximum value within a distance of \sim 0.1 μ m. Scattering of the electron beam within the TEM specimen should therefore have some influence on extracted values for Leff. Apart from grain boundary 3 in Table 1 the reduced recombination velocity of CdTe grain boundaries is more than an order or magnitude larger than the average for CST boundaries, i.e. $S_{red} = 2.63$. The large variation in the extracted values supports the conclusion that significant grain boundary passivation occurs in CST over and above CdTe.

The recombination velocity is a measure of the carrier 'lifetime' at a grain boundary; the larger its value the stronger the recombination and therefore more harmful to device performance. Many of the grain boundaries deep within the CST layer show too little contrast to carry out a meaningful quantitative analysis. We have nevertheless been able to analyse grain boundaries in the regions with intermediate selenium concentration, where the contrast is slightly higher. The results indicate that grain boundary recombination in the intermediate CST layer can be an order of magnitude lower than some CdTe grain boundaries. The true value would be even smaller for CST grain boundaries with high selenium concentration. It should be noted that grain boundary projected width does not have a large effect on grain boundary contrast in the CdTe since the CL resolution is governed by the effective carrier diffusion length, which is ~100 nm even for TEM-CL (see Tables 1 and 2).

One feature of the STEM-CL map in Fig. 2d is that the bulk CST material does not show brighter CL signal than the CdTe bulk, as would be expected from our previous SEM-CL measurements. We believe that this is because of the proximity of the free surfaces of the TEM lamella, which are separated by ~125 nm. In this situation, any increase in the carrier diffusion length caused by selenium alloying only makes it more likely that the generated carriers will diffuse to the lamella surfaces and be quenched. This highlights one disadvantage of STEM-CL, which is the proximity of the ion milled lamella surfaces, and suggests that lamella surface passivation, perhaps with alumina, could be a good way to improve STEM-CL imaging further [34]. Despite this, our other STEM-CL measurements of bilayer films have shown the expected brighter luminescence in the CST layer. One of these is shown in Fig. S3 in the Supplementary information. It can be seen that as well as having brighter CST compared to CdTe, the width of the grain boundary contrast is thinner in the CST than the CdTe, as we have seen in Fig. 2. In addition, another example of a measurement showing brighter CST is shown in Fig. 4a in the next section. It could be argued that the thin grain boundary contrast observed for CST is an artefact of electron beam injection, since the doping concentration is likely to be different between the CdTe and CST layers. The fact that these thicker specimens with brighter CL signal for the CST layer also show thin grain boundary

contrast effectively rules out electron beam injection artefacts. The thicker specimens have higher injection levels due to the incident electron beam losing more of its energy and due to the diminished role of free surface recombination. Despite this there is still a clear difference between CdTe and CST grain boundary contrast, indicating that it is a real effect.

2.3. Hyperspectral STEM-CL

A panchromatic map of the CL signal intensity over a treated bilayer cross-section, from the same device as that in Fig. 2 but taken from a different area of the film, is shown in Fig. 4a. Lower CL signal is seen at the top of the film in the CdTe, and higher signal in the CST, and there is a thick region of grain boundary contrast in the CdTe. A lowtemperature hyperspectral CL map, where a full luminescence spectrum is collected in each step of the electron beam raster, was performed on this sample. Fig. 4b shows a comparison of the average CL spectrum in the CdTe part of the sample (black curve) with the average spectrum in the CST part of the sample (blue curve). The CdTe spectrum shows a sharp excitonic peak at 1.59 eV and a broader peak at 1.43 eV, which we attribute to donor-acceptor-pair (DAP) emission [35]. The CST spectrum has similar excitonic and DAP peaks, but their peak maxima are red-shifted to lower energies (1.49 eV and 1.29 eV respectively). This is due to the band gap narrowing that occurs when CdTe is alloyed with selenium [14,36,37]. The total CL signal in the CdTe region is small at 1.1×10^6 counts, compared to 9.5×10^6 counts over the same area in the CST. In order to more directly compare the shapes and positions of the excitonic and DAP peaks for both materials, in Fig. 4c we have superimposed the spectra such that both the DAP peaks are normalised and centred at a common photon energy. It can be seen from the figure that the energy difference between the DAP and excitonic peaks is larger in the CST than in the CdTe (0.2 eV vs 0.16 eV). Since the excitonic binding energy will be similar in materials with similar relative permittivity, this indicates that DAP emission in CST material is from deeper donor and acceptor states than in CdTe. This could either be because the deeper defects are not present in CdTe, or because they are present but not undergoing radiative recombination like they are in CST. In addition, the normalised DAP peak is broader in the CST spectrum than in the CdTe, with a FWHM 43% larger. This again suggests that the addition of selenium to CdTe increases the density of donor and acceptor defects. Finally the CL spectra in Fig. 4 show only a weak transition radiation signal [26] compared to luminescence generated by electron-hole pair recombination. In Ref. [26] transition radiation was found to dominate the TEM-CL signal in CdTe. The fact that this is not the case for our samples is due to the cryogenic cooling of the specimen, and improved specimen preparation (i.e. less ion beam damage) from xenon FIB-milling. Reference [26] on the other hand used conventional gallium ion beam milling at room temperature. The suppression of transition radiation artefacts is crucial for the correct interpretation of grain boundary contrast in this work.

3. Discussion

The results presented here show that in CdCl₂ treated, selenium-graded CdTe cells there are significantly lower levels of non-radiative recombination at CST grain boundaries compared to CdTe boundaries. This suggests that selenium has a passivation effect on grain boundaries in CST material, in addition to what can already be achieved with chlorine passivation [6]. Alongside the grain interior passivation effect that has recently been discovered, the result provides an explanation for the superior carrier lifetimes and performance of selenium-alloyed CdTe. In addition, the results show that the more selenium that is present around the boundaries, the stronger the passivation effect at the boundary. This suggests that a selenium concentration above 10 at% at grain boundaries could have a stronger passivation effect than is already achieved and could lead to higher efficiency devices. It also suggests that

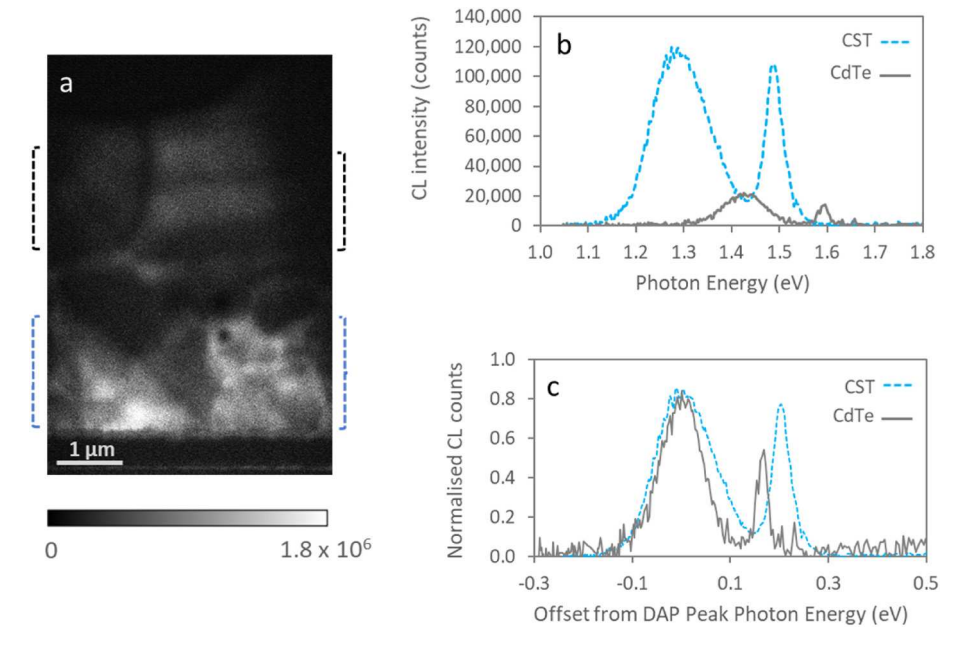


Fig. 4. (a), Low-temperature STEM-based CL map (-169.7 °C) of the total, background-corrected luminescence intensity over a cross-section of the treated CST/CdTe device, showing a brighter CST layer. Black and blue brackets respectively show the pixels that are averaged to produce the 'CdTe' and 'CST' CL spectra in (b) and (c). (b), Comparison of the average CL spectrum from the CdTe layer of the cross section versus the spectrum from the CST layer. (c), Normalised plot of the CdTe and CST spectra, with the DAP peaks centred on a common photon energy. (For interpretation of the references to colour in this figure legend, the reader is referred to the Web version of this article.)

if more selenium can be incorporated at grain boundaries at the back of the device, in the nominally CdTe region, then the amount of non-radiative carrier recombination in the absorber can be reduced and efficiencies increased (or, the CdTe layer could be removed entirely). This could be achieved by performing selenization treatments on the absorber to diffuse extra selenium into the grain boundaries.

In terms of the potential passivation mechanisms, it is not clear to what extent the reduced recombination is due to either: 1) the presence of selenium in the bulk material immediately either side of the grain boundaries, changing the electronic band structure that the boundary defects exist within; or 2) whether selenium interacts with the boundary defects themselves (i.e. selenium interacting directly with the wrong/dangling bonds); or a combination of the two. If there is no segregation of selenium at the CST grain boundaries (we could not detect any with TEM-EDX line scans) then it is worth noting that only ~ 1 in 10 of the atoms at the boundaries in our CST layer will be selenium, which corresponds to a density of 0.7-1.1 Se atoms per nm² on the boundary plane. This compares to a chlorine density of 0.8-2.0 atoms per nm² at CdCl₂ treated CdTe grain boundaries, which has been measured using SIMS [8].

4. Conclusion

In summary, in this work we have successfully performed TEM-based cathodoluminescence imaging on a selenium-graded CdTe solar cell by using xenon ion milling and sample cooling to significantly increase the luminescence signal from the TEM foil. The results show that selenium reduces harmful non-radiative recombination at grain boundaries in alloyed Cd(Se,Te) material (CST), which helps to explain the superior carrier lifetimes and record performance of selenium graded CdTe solar cells. This could lead to further efficiency improvement of CdTe-based solar cells if selenium concentrations at boundaries in the CdTe or CST parts of the absorber can be increased, or if the CdTe layer could be removed entirely to leave a purely CST absorber. In addition, the results demonstrate that TEM-CL has the potential to become a more standard technique for characterising solar cells, enabling a full package of microstructural, chemical and electronic characterisation at high resolution.

5. Experimental section

5.1. Solar cell fabrication

The two cells used in this study were deposited on TEC10 glass substrates supplied by NSG Pilkington. The substrates comprise 3 mm soda lime glass with a 400 nm fluorine doped SnO₂ transparent conducting oxide (TCO). Initially, a 100 nm MgZnO buffer layer (11% MgO, 89% ZnO) was deposited on the TCO by magnetron sputtering. This was followed by \sim 1.5 μm of CST deposited using Colorado State University's ARDS close space sublimation system [38]. During CST deposition a graphite source containing 40% CdSe was held at 575 °C, while the substrate was held at 420 °C. A ~3 µm layer of CdTe was then deposited with the CdTe source material held at 555 $^{\circ}$ C and the substrate at 500 $^{\circ}$ C (the CdTe and CST source material was supplied by 5 N Plus). One of the cells then underwent a cadmium chloride activation process. During the process a CdCl2 vapour was sublimated on to the back surface of the CdTe while the substrate was maintained at 430 °C for 600 s. It then went through a 110 s cooling step whilst held at 180 °C, removed from the vapour. Both devices then underwent a 110s copper doping treatment where copper chloride was deposited onto the back surface of the CdTe whilst held at 140 °C. The copper was then diffused into the device by a 220 $^{\circ}$ C, 220s anneal in vacuum. 30 nm of tellurium was then deposited onto the CdTe to form the back contact. The efficiency of the CdCl₂ treated device was measured at 16.8% (J_{SC} 26.8 mA/cm², V_{OC} 842 mV, Fill Factor 74.5%). The efficiency of the untreated device was measured at 0.01% (J_{SC} 0.1 mA/cm², V_{OC} 387 mV, Fill Factor 34.1%).

5.2. Transmission electron microscopy

The TEM lamellae for each sample were prepared by xenon ion milling in a FEI Helios Plasma-FIB using a standard in-situ lift out technique [12]. During final thinning the beam energy was 5 kV. STEM-CL was carried out in a JEOL 2100F FEG TEM at Brunel University. For the CL measurements the lamellae were cryogenically cooled to minus $\sim\!170~^{\circ}\text{C}$ using liquid nitrogen. The microscope is fitted with a Gatan Vulcan CL system that has two parabolic mirrors, one either side of the TEM foil. A photomultiplier tube was used for acquiring the panchromatic CL images, and a CCD camera for the spectrum images. The electron beam energy during the CL measurements was 80 kV. Due to the positioning of the parabolic mirrors of the CL holder, combined

CL-EDX measurements were not possible, hence STEM-EDX imaging was performed separately. TEM and STEM-EDX measurements were carried out in a JOEL 2000FX TEM fitted with a Oxford Instruments EDX detector.

Declaration of competing interest

The authors declare that they have no known competing financial interests or personal relationships that could have appeared to influence the work reported in this paper.

Acknowledgements

The authors at Loughborough University are grateful to the EPSRC CDT in New and Sustainable Photovoltaics for providing T.F. with a studentship, RCUK for providing funding through the EPSRC SUPERGEN SuperSolar Hub (EP/J017361/1), and the Loughborough Materials Characterisation Centre for access to the Helios PFIB, funded by the EPSRC grant EP/P030599/1. The authors at Colorado State University acknowledge support from NSF AIR, NSF I/UCRC and DOE SIPS programmes. The work at Colorado State University was supported by NSF award 1540007, NSF PFI:AIR-RA programme 1538733 and DOE SIPS award DE-EE0008177.

Appendix A. Supplementary data

Supplementary data to this article can be found online at https://doi.org/10.1016/j.solmat.2022.111595.

References

- M. Gloeckler, I. Sankin, Z. Zhao, CdTe solar cells at the threshold to 20% efficiency, IEEE J. Photovoltaics 3 (4) (Oct. 2013) 1389–1393, https://doi.org/10.1109/ JPHOTOV 2013 2278661
- [2] C. Hagenorf, M. Ebert, M. Raugei, D. Lincot, J. Bengoechea, M. Rodriguez, Cener Report Number 30.2945.0-01: Assessment of Performance, Environmental, Health and Safety Aspects of First Solar's CdTe PV Technology, 2017. https://www.cener. com/wp-content/uploads/2017/03/30.2945.0-01-FirstSolar_EUReviewReport.pdf.
- [3] M.A. Green, E.D. Dunlop, J. Hohl-Ebinger, M. Yoshita, N. Kopidakis, A.W.Y. Ho-Baillie, Solar cell efficiency tables (Version 55), Prog. Photovoltaics Res. Appl. 28 (1) (2020) 3–15, https://doi.org/10.1002/pip.3228.
- [4] R. Venkatasubramanian, et al., 18.2% (AM1.5) efficient GaAs solar cell on optical-grade polycrystalline Ge substrate, in: In Conference Record Of the Twenty Fifth IEEE Photovoltaic Specialists Conference 1996, 1996, pp. 31–36, https://doi.org/10.1109/PVSC.1996.563940.
- [5] J. Benick, et al., High-efficiency n-type HP mc silicon solar cells, IEEE J. Photovoltaics 7 (5) (Sep. 2017) 1171–1175, https://doi.org/10.1109/ JPHOTOV.2017.2714139.
- [6] J. Moseley, et al., Recombination by grain-boundary type in CdTe, J. Appl. Phys. 118 (2015), https://doi.org/10.1063/1.4926726.
- [7] A. Abbas, et al., The effect of cadmium chloride treatment on close-spaced sublimated cadmium telluride thin-film solar cells, IEEE J. Photovoltaics 3 (4) (2013) 1361–1366, https://doi.org/10.1109/JPHOTOV.2013.2264995.
- [8] D. Mao, C.E. Wickersham, M. Gloeckler, Measurement of chlorine concentrations at CdTe grain boundaries, IEEE J. Photovoltaics 4 (6) (2014) 1655–1658, https://doi. org/10.1109/JPHOTOV.2014.2357258.
- [9] J.D. Major, Grain boundaries in CdTe thin film solar cells: a review, Semicond. Sci. Technol. 31 (9) (2016) 93001, https://doi.org/10.1088/0268-1242/31/9/093001.
- [10] C.-J. Tong, K.P. McKenna, Passivating grain boundaries in polycrystalline CdTe, J. Phys. Chem. C 123 (39) (2019) 23882–23889, https://doi.org/10.1021/acs. ipcc.0b08273
- [11] E.S. Barnard, et al., 3D lifetime tomography reveals how CdCl2 improves recombination throughout CdTe solar cells, Adv. Mater. 29 (3) (2017), https://doi. org/10.1002/adma.201603801.
- [12] Ali Abbas, The Microstructure of Thin Film Cadmium Telluride Photovoltaic Materials, Loughborough University. Thesis, 2014. https://hdl.handle.net/2 134/16389.
- [13] T.A.M. Fiducia, et al., Large area 3D elemental mapping of a MgZnO/CdTe solar cell with correlative EBSD measurements, in: In WCPEC 2018 - A Joint Conference of 45th IEEE PVSC, 28th PVSEC and 34th EU PVSEC, 2018, pp. 1702–1706, https://doi.org/10.1109/PVSC.2018.8547876.
- [14] T.A.M. Fiducia, et al., Understanding the role of selenium in defect passivation for highly efficient selenium-alloyed cadmium telluride solar cells, Nat. Energy 4 (6) (Jun. 2019) 504–511, https://doi.org/10.1038/s41560-019-0389-z.

- [15] T.A.M. Fiducia, et al., "Defect tolerance in as-deposited selenium-alloyed cadmium telluride solar cells, in: IEEE 7th World Conference on Photovoltaic Energy Conversion (WCPEC) (A Joint Conference of 45th IEEE PVSC, 28th PVSEC & 34th EU PVSEC), Jun. 2018, 2018, pp. 127–130, https://doi.org/10.1109/ PVSC.2018.8547294.
- [16] D. Kuciauskas, J. Moseley, P. Ščajev, D. Albin, Radiative efficiency and charge-carrier lifetimes and diffusion length in polycrystalline CdSeTe heterostructures, Phys. Status Solidi Rapid Res. Lett. 1900606 (2019) 1–6, https://doi.org/10.1002/pssr 201900606
- [17] P. Ščajev, et al., Excitation-dependent carrier lifetime and diffusion length in bulk CdTe determined by time-resolved optical pump-probe techniques, J. Appl. Phys. 123 (2) (2018), https://doi.org/10.1063/1.5010780.
- [18] J. Moseley, et al., Cathodoluminescence analysis of grain boundaries and grain interiors in thin-film CdTe, IEEE J. Photovoltaics 4 (6) (2014) 1671–1679, https://doi.org/10.1109/JPHOTOV.2014.2359732.
- [19] J. Guo, et al., Effect of selenium and chlorine co-passivation in polycrystalline CdSeTe devices, Appl. Phys. Lett. 115 (15) (2019), https://doi.org/10.1063/ 1.5123169
- [20] J. Guo, et al., Study of effects of Cl and Se in CdSeTe solar cells using scanning transmission electron microscopy, Microsc. Microanal. 25 (S2) (2019) 2150–2151, https://doi.org/10.1017/s1431927619011486.
- [21] R. Wang, M. Lan, S.H. Wei, Enhanced performance of Se-Alloyed CdTe solar cells: the role of Se-segregation on the grain boundaries, J. Appl. Phys. 129 (2) (2021), https://doi.org/10.1063/5.0036701.
- [22] A. Shah, et al., Understanding the copassivation effect of Cl and Se for CdTe grain boundaries, ACS Appl. Mater. Interfaces 13 (29) (Jul. 2021) 35086–35096, https://doi.org/10.1021/acsami.1c06587.
- [23] X. Zheng, et al., Recombination and bandgap engineering in CdSeTe/CdTe solar cells, APL Mater. 7 (7) (2019) 71112, https://doi.org/10.1063/1.5098459.
- [24] M. Amarasinghe, D. Albin, D. Kuciauskas, J. Moseley, C.L. Perkins, W.K. Metzger, Mechanisms for long carrier lifetime in Cd(Se)Te double heterostructures, Appl. Phys. Lett. 118 (21) (2021) 211102, https://doi.org/10.1063/5.0047976.
- [25] M. Kociak, L.F. Zagonel, Cathodoluminescence in the scanning transmission electron microscope, Ultramicroscopy 176 (2017) 112–131, https://doi.org/ 10.1016/j.ultramic.2017.03.014.
- [26] B.G. Mendis, A. Howkins, D. Stowe, J.D. Major, K. Durose, The role of transition radiation in cathodoluminescence imaging and spectroscopy of thin-foils, Ultramicroscopy 167 (2016) 31–42, https://doi.org/10.1016/j. ultramic.2016.05.002.
- [27] X. Zheng, E. Colegrove, J.N. Duenow, J. Moseley, W.K. Metzger, Roles of bandgrading, lifetime, band alignment, and carrier concentration in high-efficiency CdSeTe solar cells, J. Appl. Phys. 128 (5) (Aug. 2020) 53102, https://doi.org/ 10.1063/5.0013726.
- [28] A.H. Munshi, et al., Effect of CdCl 2 passivation treatment on microstructure and performance of CdSeTe/CdTe thin-film photovoltaic devices, Sol. Energy Mater. Sol. Cells 186 (May) (2018) 259–265, https://doi.org/10.1016/j. solmat.2018.06.016.
- [29] T. Bidaud, J. Moseley, M. Al-jassim, M. Amarasinghe, W.K. Metzger, Spatially and spectrally resolved defects in polycrystalline CdTe thin films revealed by quantitative cathodoluminescence, in: 2019 IEEE 46th Photovoltaic Specialists Conference, PVSC), 2019, pp. 1–4, https://doi.org/10.1109/ PVSC40753.2019.9198976.
- [30] J. Moseley, et al., Luminescence methodology to determine grain-boundary, grain-interior, and surface recombination in thin-film solar cells, J. Appl. Phys. 124 (11) (2018), https://doi.org/10.1063/1.5042532.
- [31] T.A.M. Fiducia, et al., Three-Dimensional Imaging of Selenium and Chlorine Distributions in Highly Efficient Selenium-Graded Cadmium Telluride Solar Cells," *IEEE J. Photovoltaics*, 2019, pp. 1–5, https://doi.org/10.1109/ JPHOTOV.2019.2955313.
- [32] B.G. Mendis, L. Bowen, Q.Z. Jiang, A contactless method for measuring the recombination velocity of an individual grain boundary in thin-film photovoltaics, Appl. Phys. Lett. 97 (9) (2010), https://doi.org/10.1063/1.3486482, 0-3.
- [33] Y. Yoon, et al., Unveiling defect-mediated charge-carrier recombination at the nanometer scale in polycrystalline solar cells, ACS Appl. Mater. Interfaces 11 (50) (2019) 47037–47046, https://doi.org/10.1021/acsami.9b14730.
- [34] B. Bissig, et al., On a better estimate of the charge collection function in CdTe solar cells: Al2O3 enhanced electron beam induced current measurements, Thin Solid Films 633 (2017) 218–221, https://doi.org/10.1016/j.tsf.2016.08.012.
- [35] V. Consonni, G. Feuillet, S. Renet, Spectroscopic analysis of defects in chlorine doped polycrystalline CdTe, J. Appl. Phys. 99 (5) (2006), https://doi.org/10.1063/ 1.2174117.
- [36] D.E. Swanson, J.R. Sites, W.S. Sampath, Co-sublimation of CdSe x Te 1 À x layers for CdTe solar cells, Sol. Energy Mater. Sol. Cells 159 (2017) 389–394, https://doi. org/10.1016/j.solmat.2016.09.025.
- [37] M.J. Watts, T.A.M. Fiducia, B. Sanyal, R. Smith, J.M. Walls, P. Goddard, Enhancement of photovoltaic efficiency in CdSe x Te 1-x (where $0 \le x \le 1$): insights from density functional theory, J. Phys. Condens. Matter 32 (12) (Mar. 2020) 125702, https://doi.org/10.1088/1361-648X/ab5bba.
- [38] D.E. Swanson, et al., Single vacuum chamber with multiple close space sublimation sources to fabricate CdTe solar cells, J. Vac. Sci. Technol. A Vacuum, Surfaces, Film. 34 (2) (2016) 21202, https://doi.org/10.1116/1.4941071.